RSC Advances

PAPER

View Article Online
View Journal | View Issue

Cite this: *RSC Adv.*, 2020, **10**, 2944

Platinized agarose microspheres as a new modifier in graphite paste electrodes for the electrochemical determination of 4-aminophenol

M. Tohidinia, *[a] A. Biabangard[a] and M. Noroozifar[b]

In the environment, 4-aminophenol (4-AP) is present as a highly toxic compound and water pollutant. In this study, platinized agarose microspheres (PtAM) were used for the first time, for the preparation of a novel, modified graphite paste electrode (GPE/PtAM) for the electrochemical determination of 4-AP. PtAM was characterized using transmission electron microscopy, field emission scanning electron microscopy and energy dispersive X-ray analysis. The electrochemical response characteristics of GPE/PtAM towards 4-AP were investigated *via* electrochemical impedance spectroscopy, cyclic voltammetry, differential pulse voltammetry and chronoamperometry. The value of the charge transfer resistance obtained for GPE/PtAM was 27.3 Ω. Microscopic surface areas and the surface concentration of the electroactive species for GPE/PtAM were calculated to be 0.077 cm^2 and 1.13 × 10^{-3} mol cm^{-2}, respectively. The electron transfer coefficient, diffusion coefficient and standard heterogeneous rate constants of 4-AP were calculated as 0.274, 4.56 × 10^{-4} cm^2 s^{-1}, and 3.32 × 10^{-1} cm s^{-1}, respectively. The influence of pH on the oxidation of 4-AP was investigated and a pH value of 2.0 (using a phosphate buffer solution) was selected as the optimum pH. Under optimum conditions, the calibration was linear between 0.8 and 87 μM with a detection limit of 45 nM. Moreover, GPE/PtAM was applied to determine the concentrations of 4-AP in water samples with satisfactory results.

Received 22nd October 2019
Accepted 15th December 2019

DOI: 10.1039/c9ra08629c

rsc.li/rsc-advances

1 Introduction

Phenol compounds such as aminophenols are dangerous environmental contaminants which are used extensively as industrial raw or processed materials in cosmetics, photograph development, dyestuffs, chemical inhibitors, and petroleum additives. Most of them can remain in the environment for a long time with high toxicity and carcinogenicity, because of their stability and bio-accumulation. Among them, 4-AP is also used in the pharmaceutical industry for the production of paracetamol, but it is highly toxic. The maximum content of 4-AP in pharmaceuticals is limited to 50 ppm (0.005%, w/w) by the standards of the European, United States, and Chinese pharmacopoeias.[1] Phenols are ubiquitous environmental pollutants.[2] In particular, 4-AP is considered to be one of priority toxic pollutants.[3] Therefore, it is necessary to develop simple and reliable methods for determination of 4-AP, for environmental protection and food security. Many attempts, therefore, have been made to develop an efficient and selective way of determining 4-AP, such as liquid chromatography,[4,5] spectrophotometry,[6] sequential injection analysis,[7] capillary electrophoresis,[8] and micellar electrokinetic chromatography.[9] However, use of these techniques suffer because they are expensive and have a long analysis time. An electrochemical technique, with a low cost, simplicity, and high selectivity and sensitivity, is a desired method for 4-AP detection. Different electrodes have been made to identify and measure aminophenol.[1,10–13] An agarose is a polysaccharide polymer material, commonly extracted from seaweed (Scheme 1). Agarose, a kind of natural polysaccharide, has been widely used for immobilization of enzymes, antibodies and chemical molecules due to its attractive properties of excellent film-forming ability, biocompatibility, non-toxicity, high mechanical strength and inexpensiveness.[14–16] Agarose is an ideal biopolymer to use for immobilization of materials on solid substrates. Its application in direct electrochemistry was reported previously.[17] Metal nanoparticles such as platinum nanoparticles (PtNPs) offer a wide range of chemo-physical properties that can be of interest for many technological applications due to their catalytic activity, electrochemical applications, and chemical sensing.[18] So, Pt is used in electrochemical measurements.[19,20] In previous research, Pt or its composite with different supports were used for oxidation of low molecular fuels and in fuel cells.[21–24] In the present study, platinized agarose microspheres (PtAM) were used for the first-time as a novel modifier for the preparation of a modified graphite paste electrode for the electrochemical determination of 4-AP. As far as is known, no previous study has reported using PtAM in any electrochemical determination. Platinized microspheres can act as tiny

[a]*Department of Chemistry, University of Sistan and Baluchestan, Iran*
[b]*University of Toronto, Canada. E-mail: tohidiniamasoumeh@gmail.com*

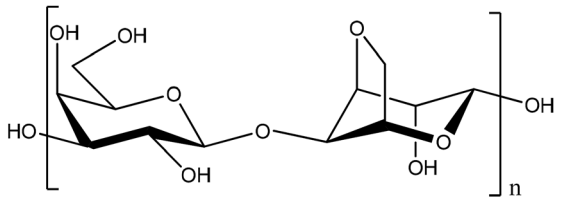

Scheme 1 The structure of agarose.

conduction centers to facilitate electron transfer by giving more freedom to the immobilized biomolecules, which brings the active sites closer to the electrode surface.[25,26] This polymer is a bio-molecular polymer with a high mechanical strength and has been used for sensitive and selective determination of these analytes.[27] The results showed low detection limits and excellent selectivity. In addition, the proposed method was successfully applied for the determination of 4-AP in water samples.

2 Experimental

2.1. Reagents

Agarose, 4-AP, ethanol, hexachloroplatinic acid hexahydrate, hydrazine hydrochloride, sodium hydroxide, hydrogen chloride, phosphoric acid, potassium dihydrogen phosphite, potassium hydrogen phosphite, graphite powder and paraffin oil were purchased from the Merck Company. All reagents were analytical grade and were used as received without any purification. All solutions were prepared with ultra-pure Milli-Q water (UPM-Q) with a resistivity of 18.2 mW cm and purged with pure nitrogen gas (99.999%) before the investigations.

2.2. Apparatus

Cyclic voltammetry (CV), and differential pulse voltammetry (DPV) were carried out on a potentiostat/galvanostat (SAMA 500 electroanalyzer system, Iran) with a three-electrode system that use a modified electrode as the working electrode, a Pt electrode as the counter electrode and a saturated calomel electrode as the reference electrode. Electrochemical impedance spectroscopy (ESI) was performed with a potentiostat/galvanostat (Autolab/PGSTAT128N, Eco Chemie, Netherlands) controlled by NOVA 1.11 software (Metrohm Autolab). Electrochemical impedance measurements were performed in 5 mM $[Fe(CN)_6]^{3-/4-}$ prepared in 0.1 M KCl. The EIS was performed over a frequency range of 10 kHz to 0.1 Hz with a 10 mV amplitude and it was superimposed on the formal potential of the redox probe ($E'_0 = E^{1/2} = (E_{Pa} + E_{Pc})/2$, when $D_{ox} = D_{red}$) which was calculated from the cyclic voltammograms. The field emission scanning electron microscopy (FESEM) was carried out using an electron microscope (MIRA3, Tescan) and energy dispersive X-ray analysis (EDX) was carried out using an electron microscope (SAMx, France). Transmission electron microscopy (TEM) images were taken using a transmission electron microscope (CM120, Philips) with 2.5 Å resolution. The pH measurements were made using a pH meter (model 744, Metrohm). All experiments were performed at room temperature (RT).

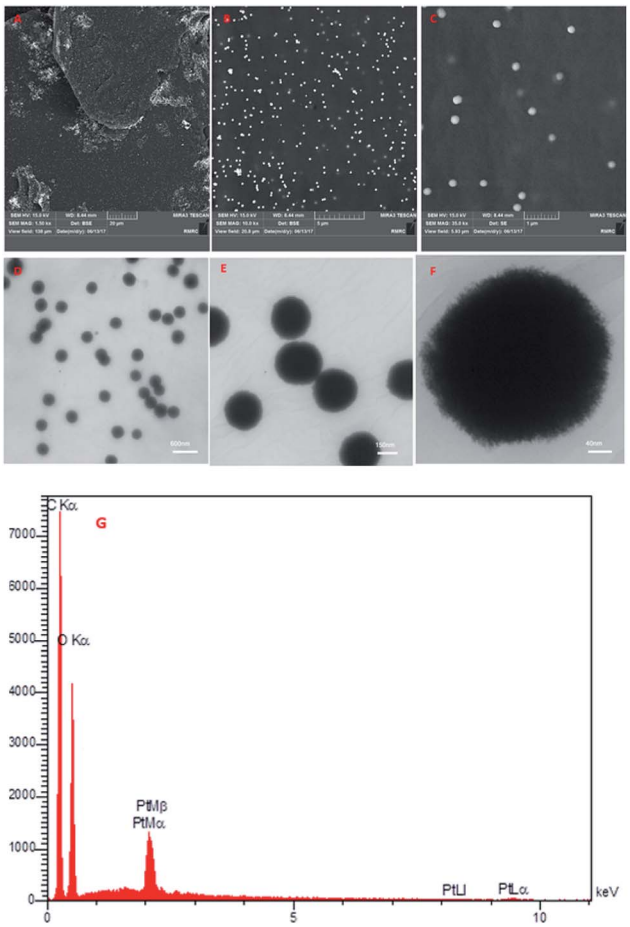

Fig. 1 (A–C) FESEM images of PtAM, (D–F) TEM images of PtAM, and (G) EDX analysis of PtAM.

2.3. Preparation of experimental solutions

The solution of Pt^{4+} (0.01 M) was prepared by dissolving the hexachloroplatinic acid hexahydrate in UPM-Q. The hydrazine solution (0.01 M) was prepared by dissolving hydrazine in UPM-Q. The stock solutions of 4-AP (0.01 M) were prepared by dissolving the solid in a small volume of 0.1 mol L^{-1} ethanol solution then diluted with UPM-Q to give the final concentration. Phosphate buffer solution (PBS) was prepared from phosphoric acid (0.2 M), and the pH range was adjusted to 2.0–9.0 with 0.2 M phosphoric acid and 0.2 M sodium hydroxide solutions and these PBS solutions were used as the supporting electrolytes. All experiments were performed under a nitrogen atmosphere at RT.

2.4. Preparation of a modified graphite paste electrode with PtAM

The PtAM was prepared by mixing 0.09 g agarose with 2.5 ml of a 0.01 M Pt^{4+} solution. The mixture was stirred for 20 min and then a solution of 0.01 M hydrazine was added to this mixture at RT. With addition of hydrazine, the solution color changed from orange to black, which represented a reduction of the platinum ions to platinum (eqn (1)). The platinum atoms sit around the hydroxyl agarose groups, which caused nucleation and lead to the small, spherical nanoparticles shown in Fig. 1.

$$Pt^{4+} + N_2H_5^+ \rightarrow Pt + N_2 + 5H^+ \quad (1)$$

Then PtAM solution was centrifuged, and the black precipitate was washed with deionized water and air dried for 24 h. The GPE/PtAM was prepared by mixing 0.006 g of PtAM, 0.194 g of graphite powder and 0.4 mL paraffin oil using a mortar and pestle. The mixture was ground for 20 min until a uniform paste was obtained. The resulting paste was then inserted into the bottom of a glass tube with an internal diameter of 4 mm and a length of 8 cm. Electrical connection was implemented by a copper wire lead fitted into the glassy tube. When necessary, a new surface was obtained by pushing some of the paste out of the tube and polishing the end with a weighing paper. Moreover, the GPE/A was prepared in the same way without adding Pt to the mixture and unmodified GPE was prepared in the same way without adding PtAM to the mixture. These GPEs were used for comparison with the GPE/PtAM.

3 Results and discussion

3.1. Morphological and energy dispersive X-ray analysis of the PtAM

The morphology of PtAM was appraised using FESEM and TEM and the results are shown in Fig. 1. From Fig. 1, the FESEM (Fig. 1A–C) and TEM (Fig. 1D–F) images of PtAM show that the mono dispersible microspheres were indeed microspherical in shape. The EDX data for PtAM revealed the presence of the expected elements, namely C, O and Pt, in the structure of PtAM (Fig. 1G). Based on the EDX and TEM results, the platinum particles were present, and doped and dispersed in the agarose microspheres with a size between 150 and 200 nm.

3.2. Electrochemical impedance spectroscopy (ESI) study

Fig. 2A shows the CVs of GPE, GPE/A and GPE/PtAM in 0.1 M KCl containing 5 mM $Fe(CN)_6^{3-/4-}$. The CV of GPE showed a $\Delta E_P(E_{Pa} - E_{Pc})$ of 0.638 V and oxidation and reduction peak currents of 7.11 μA and −7.83 μA, respectively, and the CV of GPE/A showed ΔE_P of 0.274 V and oxidation and reduction peak currents of 8.67 μA and −9.65 μA, respectively. Comparatively, the GPE/PtAM showed ΔE_P of 0.104 V and oxidation and reduction peak currents of 11.75 and −14.11 μA, respectively. This decrease in the ΔE_p and increase in the peak currents of the GPE/PtAM compared to GPE were due to the electrocatalytic activity of the hydroxyl groups which were free and unreacted in the agarose and the presence of the hydroxyl groups functionalization with Pt on the surface agarose *via* electrochemical reactions. Supporting evidence for this modified electrode was found from the EIS study, which is a powerful technique for studying electrode–electrolyte interfacial features. As shown in Fig. 2B, the Nyquist plots of these electrodes comprise two parts, one semicircle at higher frequencies which indicated charge transfer limitations and its diameter was equal to the charge transfer resistance (R_{ct}) whereas the second part of the Nyquist plot was a straight line which appeared in low frequencies and indicated the mass transfer limitations.[28] The

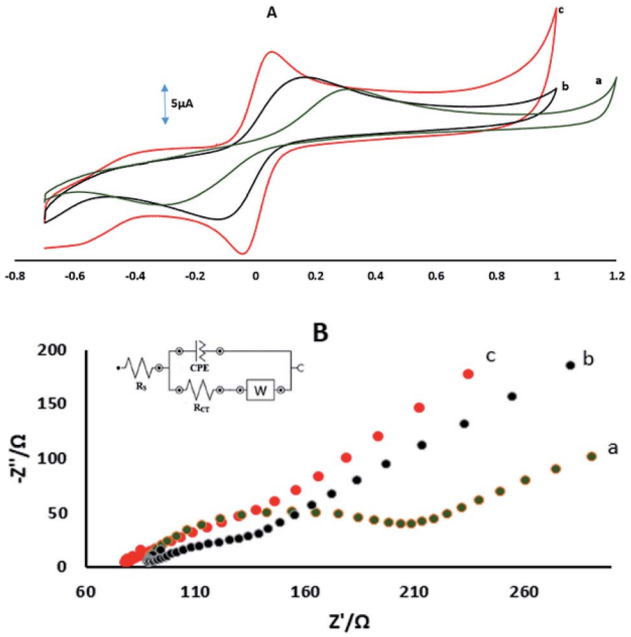

Fig. 2 (A) CVs of (a) GPE, (b) GPE/A, and (c) GPE/PtAM in 1 mM $Fe(CN)_6^{3-/4-}$ prepared in 0.1 M KCl, measured at a scan rate 100 mV s^{-1}. (B) Nyquist plots showing the step-wise modification of (a) GPE, (b) GPE/A and (c) GPE/PtAM. Electrochemical measurements were performed in 10 mM $Fe(CN)_6^{3-/4-}$ prepared in 0.1 M KCl. The EIS data was obtained over a frequency range of 0.1 Hz to 10 kHz. The inset shows the equivalent circuit. CPE: constant phase element, R_{ct}: charge transfer resistance, R_s: solution resistance, and W: Warburg element.

NOVA software was used for fitting and simulation of the EIS data whereas the modified Randles equivalent circuit, which is illustrated in the inset of Fig. 2B was selected as the equivalent circuit for fitting and simulation of the EIS data. The lower value of R_{ct} shows the easier electron transfer between the electrode surface and the probe ions ($Fe(CN)_6^{3-/4-}$). The values of R_{ct} obtained for GPE, GPE/A and GPE/PtAM were: 128.42, 53.96 and 27.32 Ω, respectively. The lower value of R_{ct} for GPE/PtAM compared to GPE was attributed to the electrocatalytic activity of the hydroxyl functional groups in agarose and the presence of Pt.

3.3. Electrochemical behaviour of the electrodes

The microscopic surface areas of GPE, GPE/A and GPE/PtAM were determined by using the Randles–Sevcik equation:[29]

$$I_{Pa} = 2.96 \times 10^5 n^{3/2} A C_0 D_R{}^{1/2} \nu^{1/2} \quad (2)$$

where I_{Pa} (μA) is the anodic peak current, n is the number of transferring electrons, A is the microscopic area (cm^2), C_0 (mM) is the bulk concentration of the probe ion, D_R is the diffusion coefficient ($cm^2\ s^{-1}$) and ν ($V\ s^{-1}$) is the scan rate. For 1 mM $Fe(CN)_6^{3-/4-}$ in 0.1 M KCl the number of transferring electrons equals one ($n = 1$) and $D_R = 7.6\ cm^2\ s^{-1}$.[30] Fig. 3 shows the CVs and the plots of I_{Pa} *vs.* $\nu^{1/2}$ for GPE, GPE/A and GPE/PtAM in the presence of 1 mM of $Fe(CN)_6^{3-/4-}$ in 0.1 M of KCl supporting electrolyte. From the slopes of the trend lines, the microscopic surface areas obtained were: 0.035, 0.042 and 0.077 cm^2 for

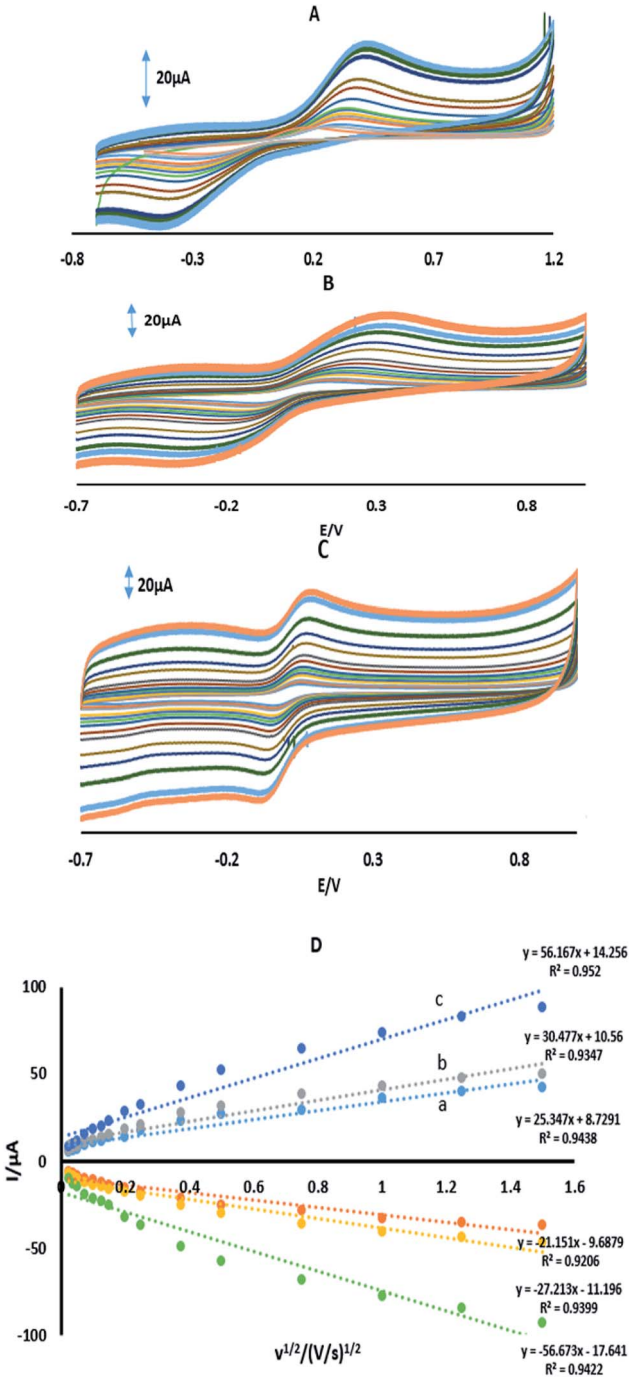

Fig. 3 CVs of (A) GPE, (B) GPE/A, and (C) GPE/PtAM in 1 mM $Fe(CN)_6^{3-/4-}$ prepared in 0.1 M KCl, and (D) the plot of peak current *vs.* the square root of scan rate for (a) GPE, (b) GPE/A and (c) GPE/PtAM.

GPE, GPE/A and GPE/PtAM, respectively. The highest microscopic surface area for GPE/PtAM was due to the presence of Pt in the microspheres. Fig. 4 shows the CVs in PBS of pH 2.0 for GPE, GPE/A and GPE/PtAM. For GPE/PtAM the field current was greater than that of both GPE/A and GPE. Fig. 4c shows the oxidation and reduction peaks of platinum.[31] An approximate amount of the electroactive species[31] can be estimated by the Sharp equation.[32] The peak current is related to the surface concentration of electroactive species, Γ, by eqn (3):

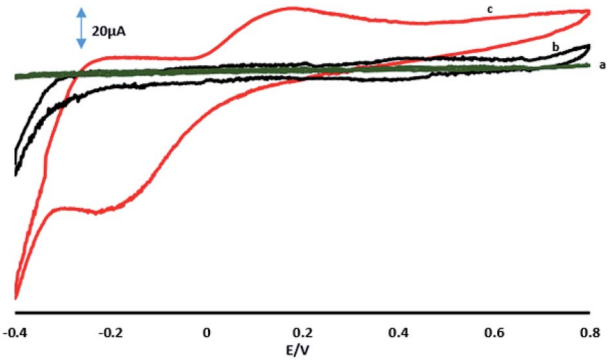

Fig. 4 CVs measured in PBS with a pH of 2.0: (a) GPE, (b) GPE/A and (c) GPE/PtAM.

$$I_p = n^2F^2A\Gamma\nu/4RT \quad (3)$$

where n represents the number of electrons involved in the reaction, A is the geometric surface area of the electrode (0.1256 cm^2), Γ is the surface concentration of the electroactive species (mol cm^{-2}), ν is the scan rate (V s^{-1}), R (8.314 J mol^{-1} K^{-1}), F (96 485 C mol^{-1}) and T (298 K) denote the gas constant, the Faraday constant, and the temperature, respectively. From the slope of the plot of the anodic peak currents *vs.* scan rates, the surface concentration of electroactive species for the GPE/PtAM was calculated to be 2.8×10^{-4} mol cm^{-2} for $n = 2$ (see Fig. 5).

3.4. Electrochemical behavior of 4-AP at different electrodes

Fig. 6A shows the CVs of 70 μM 4-AP at the surface of GPE, GPE/A and GPE/PtAM in PBS at pH 2.0. Based on the results for the

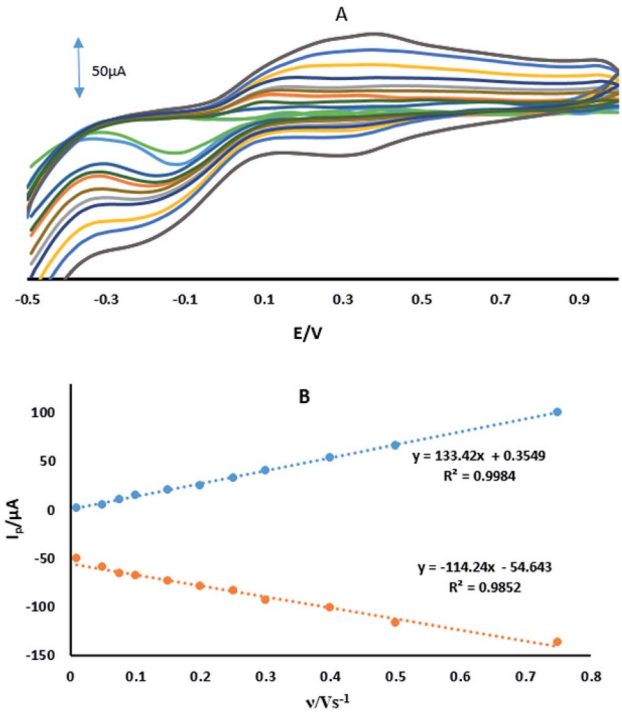

Fig. 5 (A) CVs of GPE/PtAM at different scan rates of 0.01, 0.05, 0.075, 0.1, 0.15, 0.2, 0.25, 0.3, 0.4, 0.5 and 0.75 V s^{-1}. (B) Variation of I_p *vs.* the ν.

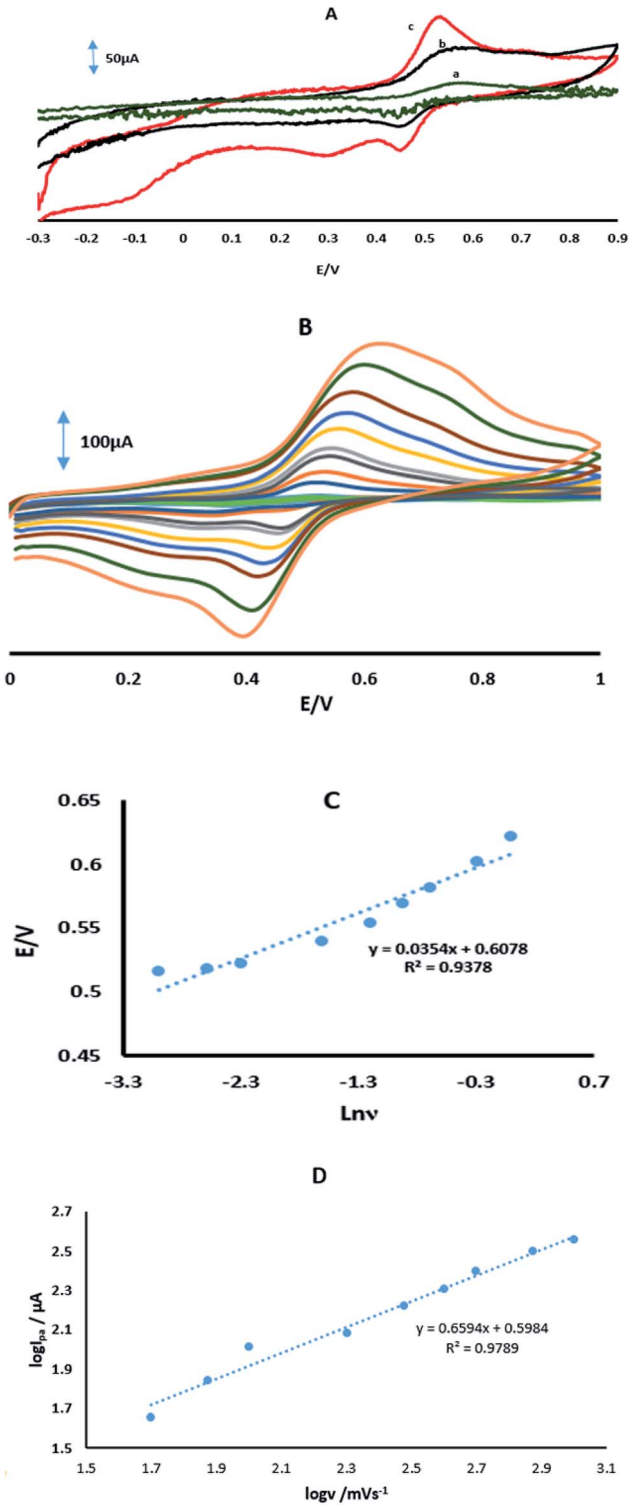

Fig. 6 (A) CVs in PBS with a pH of 2 in the presence of 70 μM 4-AP for (a) GPE, (b) GPE/A and (c) GPE/PtAM. (B) CVs of GPE/PtAM in the presence of 70 μM 4-AP at different scan rates of 0.05, 0.075, 0.1, 0.2, 0.3, 0.4, 0.5, 0.75 and 1 V s^{-1}. (c) Variation of E_p *vs.* ln ν. (D) A plot of the logarithm of the anodic peak currents *vs.* the logarithm of the scan rates.

electrodes, there was a higher peak current with a lower oxidation potential for 4-AP at the surface of GPE/PtAM, so GPE/PtAM was selected for the determination of 4-AP. The effect of scan rate on the electrochemical oxidation of 4-AP at GPE/PtAM was investigated by CV (Fig. 6B). Based on the results shown in this figure, the oxidation peak potentials for 4-AP were shifted to positive values with increasing scan rates, confirming the kinetic limitations of the electrochemical reaction. The plot of EP *vs.* ln(ν) was a straight line with a slope:[33]

$$\frac{\delta E_P}{\delta\ (\ln \nu)} = \frac{RT}{(1-\alpha)nF} \quad (4)$$

where α stands for the electron transfer coefficient, and the slope form plot E_P *vs.* ln(ν) for 4-AP was 0.0354 V (Fig. 6C). The α value for $n = 1$ and $T = 298$ K was calculated to be 0.274 for 4-AP. A linear increase in anodic peak current was observed with the increase in scan rate. A straight-line graph was obtained when the logarithms of the peak currents were plotted against the logarithms of the scan rates (Fig. 6D).

$$\log I_{Pa}\ (\mu A) = 0.6594 \log \nu + 0.5984\ (R^2 = 0.9789) \quad (5)$$

The results indicated that the electrode process was adsorption controlled rather than diffusion controlled. This could also be confirmed by the observed positive shift in the anodic peak potential with an increase in scan rate.

3.5. Chronoamperometric study

The chronoamperometry study of 4-AP at GPE/PtAM is shown in Fig. 7. As shown in this figure, the diffusion coefficients of 4-AP can be calculated by the Cottrell equation. This equation describes the variation of current with time for a diffusion controlled process:[33]

$$I_P = nFCD^{1/2}\pi^{-1/2}t^{-1/2} \quad (6)$$

where D and C are the diffusion coefficient ($cm^2\ s^{-1}$) and the concentration (mol cm^{-3}), respectively, A and F are the surface area of the working electrode (0.1256 cm^2) and the Faraday constant (96 485 C mol^{-1}), respectively. Under diffusion control

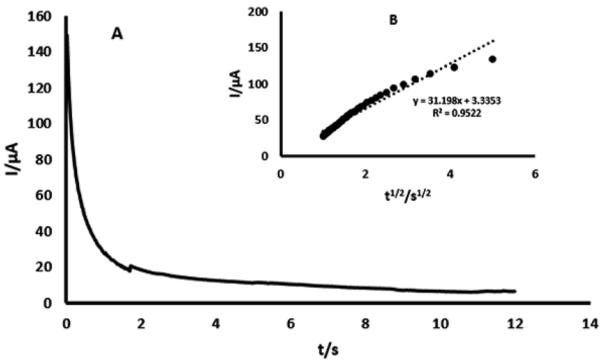

Fig. 7 (A) Chronoamperogram obtained from GPE/PtAM with PBS with a pH of 2.0 for a concentration of 0.2 mM 4-AP, (B) plots of I *vs.* $t^{-1/2}$ obtained from the chronoamperogram of 4-AP.

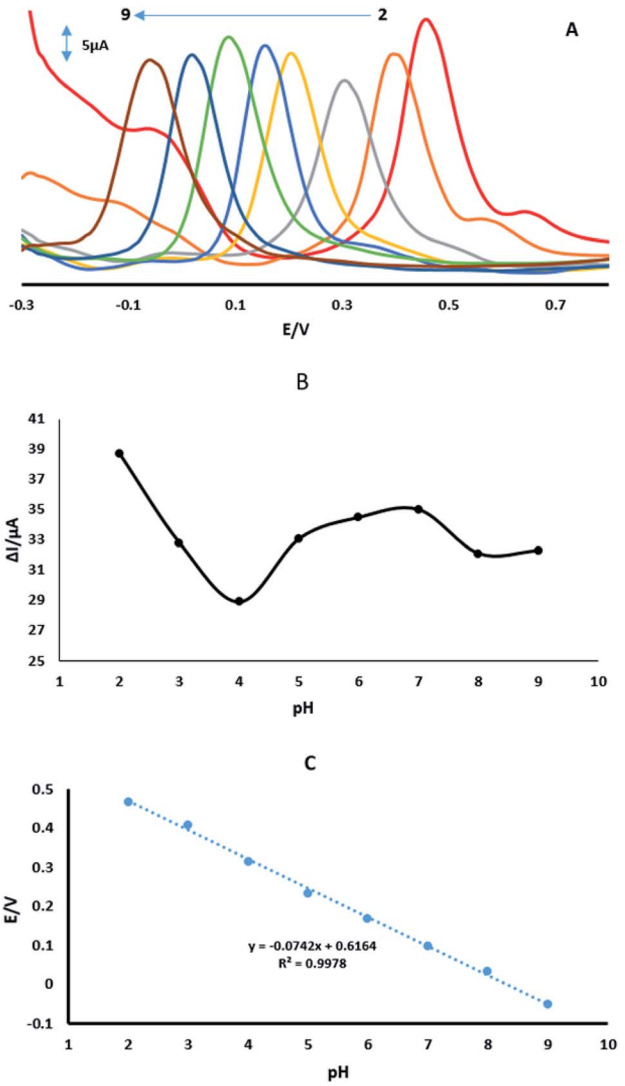

Fig. 8 (A) DPVs of GPE/PtAM with 70 μM 4-AP at a scan rate of 50 mV s^{-1} with PBS with pH values of 2.0 to 9.0. (B) Variation of ΔI_p *vs.* buffered pH. (C) Variation of E_p *vs.* buffered pH.

(mass transport), a plot of I *vs.* $t^{-1/2}$ was linear, and the value of D could be obtained from its slope. The value of D was found to be 4.56×10^{-4} cm^2 s^{-1} for 4-AP. The standard heterogeneous rate constant (K_s) for the electrochemical reactions of 4-AP at the surface of GPE/PtAM, were evaluated by CV according to the Velasco equation, as given by eqn (7):[34]

$$K_s = 1.11\ D_0^{1/2}(E_P - E_{P1/2})^{-1/2}\nu^{1/2} \quad (7)$$

where K_s refers to the standard heterogeneous rate constant (cm s^{-1}), D_0 is the diffusion coefficient (cm^2 s^{-1}), E_P and $E_{P1/2}$ refer to potential peak and potential in half of peak currents (V), respectively, and ν is the scan rate (V s^{-1}). The value of K_s was found to be 3.32×10^{-1} cm s^{-1} for 4-AP at GPE/PtAM. The K_s for GPE, was calculated to be 1.49×10^{-3} cm s^{-1}. Based on these results, the K_s value for GPE/PtAM was 222.8 times higher than that obtained with GPE. Higher K_s values gave faster electron transfer for the electrochemical reaction of 4-AP molecules at GPE/PtAM.

3.6. Influence of pH on the oxidation of 4-AP

Fig. 8A shows the effect of pH of 70 μM 4-AP in 0.1 M PBS on the GPE/PtAM with PBS at a range of pH (2.0–9.0), Fig. 8B shows the plot of oxidation peak current of analytes *vs.* pH. Based on this figure, PBS with a pH of 2.0 exhibited the maximum peak current. Therefore, pH 2.0 was selected as optimum pH for PBS. The potentials of 4-AP followed the linear regression equations (Fig. 8C) with:

$$E_p = -0.0742\ \text{pH} + 0.6164\ (R^2 = 0.9978) \quad (8)$$

According to the formula: $dE_p/d\text{pH} = 2.303\ (mRT/nF)$, where m and n were the number of protons and electrons, respectively.[30] The slope of the equation of 4-AP was close to the theoretical value of 0.059 V pH^{-1}, indicating that the electrochemical redox of 4-AP should be the same number of electrons and proton processes. This conclusion was in accordance with the known electrochemical reaction of 4-AP at the surface of GPE/PtAM with PBS at a pH of 2, which is illustrated in eqn (9):

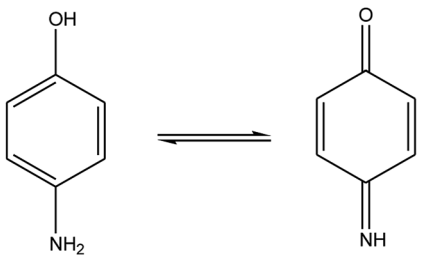

(9)

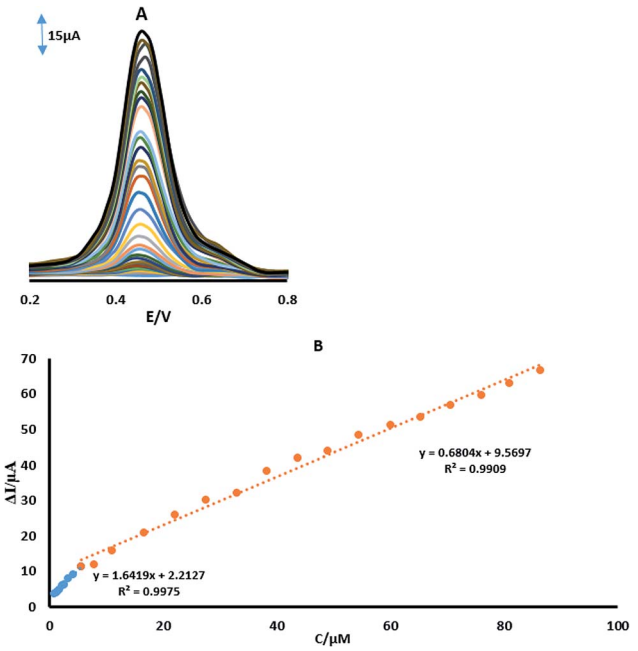

Fig. 9 (A) DPVs of GPE/PtAM in PBS with a pH of 2 containing different concentrations of 4-AP. (B) Plots of ΔI *vs.* concentration of 4-AP.

Table 1 Comparison of the manufactured electrode for 4-AP detection with electrodes used by other researchers

Entry	DL[a] (nM)	LR[b] (μM)	Ref.
PcCo/CNT/GCE[c]	300	0.5–800	1
Graphene–chitosan/GCE[d]	57	0.2–550	10
GR–PANI/GCE[e]	65	0.2–100	11
CFMEs[f]	1000	—	12
CILE[g]	100	0.3–1000	13
HRP/NPG/CPE[h]	110	5–60	35
G-PANI/CPE[i]	15 680	50–500	36
GN-CD-cMWCNT[j]	19	0.2–125	37
LC[k]	4580	45.8–366.5	5
MEKC[l]	54 970	183.2–1374.4	9
HPLC[m]	460	0.92–247.9	38
SPE-HPLC/DAD[n]	0.6	0.46–13.7	4
SPE-fast-HPLC/DAD[o]	2.5	4.6–11.4	4
IECLC/AD[p]	45	4.5–45	43
Paper-based column/AD[q]	10 000	50–2000	40
LC	640	0.92–183.3	41
MEKC	1920	4.5–549.7	41
HPLC/AD	9	0.009–18.32	42
GPE/PtAM	45	0.8–87	This work

[a] Detection limit. [b] Linear range. [c] β-[3-(Dimethylamine)phenoxy] phthalocyanine cobalt(II)-multiwalled carbon nanotube hybrid/glassy carbon electrode. [d] Graphene–chitosan/glassy carbon electrode. [e] Graphene-polyaniline/glassy carbon electrode. [f] Carbon fibre microelectrodes. [g] Carbon ionic liquid electrode. [h] Horseradish peroxidase-nanoporous gold co-catalytic strategy/carbon paste electrode. [i] Graphene-polyaniline modified carbon paste electrode. [j] Carboxyl multi walled carbon nanotube-cyclodextrin-edge functionalized graphene composite. [k] Liquid chromatography. [l] Micellar electrokinetic chromatography. [m] High-performance liquid chromatography. [n] Solid phase extraction-high-performance chromatography coupled to diode array detection. [o] Solid phase extraction-fast-high-performance chromatography coupled to diode array detection. [p] Anion exchange capillary liquid chromatography coupled to amperometric detection. [q] High-performance liquid chromatography/amperometric detection.

Table 2 Determination of 4-AP in water samples ($n = 3$)

Sample		Added (μM)		Found (μM)		Recovery (%)		RSD (%)	
Tap water	1	33	50	33.2	52.1	100.6	104.2	1.92	2.85
	2	33	50	33.9	51.4	102.7	102.8	1.86	2.62
Well water	1	33	50	32.5	48	98.4	98	2.93	1.94
	2	33	50	34.1	51.6	103.3	103.2	1.79	2.74

3.7. Linear range and detection limit oxidation of 4-AP

Differential pulse voltammetry was used for the determination of 4-AP (Fig. 9A). In order to obtain the best sensitivity under the specific conditions used, an amplitude scan rate of 50 mV s^{-1} and PBS with a pH of 2.0 were used. The response was linear with the 4-AP concentration which consisted of two linear segments with slopes of 1.6419 and 0.6804 μA μM^{-1} in the concentration ranges from 0.8 μM to 16.6 μM and 16.6 μM to 87 μM, respectively (Fig. 9B). At the low and high concentrations of the 4-AP, the surface activity of the modified electrode was different, which was responsible for the observed difference in the slopes of the two linear segments. A high number of active sites were available on the electrode surface at lower concentrations of the analytes. However, the number of active sites decreased at higher concentrations of the analytes. The different number of active sites and likely kinetic limitation resulted in the decreased sensitivity of the slope in the second linear segments for 4-AP. The detection limit was determined to be 45 nM for 4-AP on surface of GPE/PtAM. In Table 1, the results of a comparison study of the present work with some different modified electrodes[1,10–13,35–37] and different chromatography methods,[4,5,9,38–42] which show acceptable performance according to the tabulated data of this electrode. Furthermore, the interfering effects of other probable coexisting ions such as Ca^{2+}, Cl^{-}, Cr^{3+}, Cu^{2+}, K^{+}, Mg^{2+}, Na^{+}, NO_3^{-}, PO_4^{3-}, SO_4^{2-} and Zn^{2+}, were investigated and the results showed that the maximum interfering effects for these ions were seen with the determination of 4-AP (5% tolerable molar ratio >100). Moreover, no significant interfering effects were seen for these ions.

3.8. Analytical application

The practical application of GPE/PtAM was examined for the determination of 4-AP in tap water and well water. The samples were diluted with PBS (pH 2.0) and DPVs were used for the determination of 4-AP using the standard addition method. Based on the results in Table 2, the recoveries for three water samples were 98–104.2% for 4-AP. These recovery amounts were acceptable for the determination of 4-AP.

4 Conclusions

In this work, Pt was included on the surface of agarose and was used in GPEs. A modified GPE with PtAM was used for the determination of 4-AP as a water pollutant. Depending on the hydroxide groups present in the agarose structure, and the presence of Pt, the sensitivity of the electrode towards 4-AP increases. Some electrochemical measurements of the modified electrode and analyte on the surface modified electrode were studied. A value of 27.32 Ω was obtained for the charge transfer resistance of GPE/PtAM. Microscopic surface areas and the surface concentration of electroactive species for GPE/PtAM were calculated to be 0.077 cm^2 and 1.13×10^{-3} mol cm^{-2}, respectively. The electron transfer coefficient, the diffusion coefficient and the standard heterogeneous rate constant of 4-AP on GPE/PtAM were calculated as 0.274, 4.56×10^{-4} cm^2 s^{-1} and 3.32×10^{-1} cm s^{-1}, respectively. The influence of pH on the oxidation of 4-AP was investigated and PBS with a pH of 2.0 was selected as the optimum pH. Under optimum conditions, a 45 nM detection limit was obtained. The preparation method is simple and cheap, and the proposed modified electrode is very stable. Finally, GPE/PtAM was successfully used for the determination of 4-AP in real samples.

Conflicts of interest

There are no conflicts to declare.

Acknowledgements

We appreciate and acknowledge financial support from the University of Sistan and Baluchestan (USB).

References

1 L. Guo, Z. Chen, J. Zhang, H. Wu, F. Wu, C. He, B. Wang and Y. J. R. A. Wu, *RSC Adv.*, 2015, **5**, 23283–23290.
2 T. Saitoh, K. Asano and M. Hiraide, *J. Hazard. Mater.*, 2011, **185**, 1369–1373.
3 H. Kool, C. Van Kreijl, B. Zoeteman and R. Tardiff, *Crit. Rev. Environ. Sci. Technol.*, 1982, **12**, 307–357.
4 L. H. Santos, P. Paíga, A. N. Araújo, A. Pena, C. Delerue-Matos and M. Montenegro, *J. Chromatogr. B: Anal. Technol. Biomed. Life Sci.*, 2013, **930**, 75–81.
5 L. Monser and F. Darghouth, *J. Pharm. Biomed. Anal.*, 2002, **27**, 851–860.
6 G. D. Rodrigues, L. R. de Lemos, P. da Rocha Patrício, L. H. M. da Silva and M. da Silva, *J. Hazard. Mater.*, 2011, **192**, 292–298.
7 A. B. Vishnikin, M. K. Al-Shwaiyat, G. A. Petrushina, L. P. Tsiganok, V. Andruch, Y. R. Bazel, H. Sklenářová and P. J. T. Solich, *Talanta*, 2012, **96**, 230–235.
8 Q. Chu, L. Jiang, X. Tian and J. Ye, *Anal. Chim. Acta*, 2008, **606**, 246–251.
9 T. Németh, P. Jankovics, J. Németh-Palotás and H. Kőszegi-Szalai, *J. Pharm. Biomed. Anal.*, 2008, **47**, 746–749.
10 H. Yin, Q. Ma, Y. Zhou, S. Ai and L. Zhu, *Electrochim. Acta*, 2010, **55**, 7102–7108.
11 Y. Fan, J. Liu, C. Yang, M. Yu and P. Liu, *Sens. Actuators, B*, 2011, **157**, 669–674.
12 M. Jamal, A. S. Sarac and E. J. S. Magner, *Sens. Actuators, B*, 2004, **97**, 59–66.
13 A. Safavi, N. Maleki and O. Moradlou, *Electroanalysis*, 2008, **20**, 2158–2162.
14 M. Khayyami, M. T. P. Pita, N. P. Garcia, G. Johansson, B. Danielsson and P. O. Larsson, *Talanta*, 1998, **45**, 557–563.
15 X. H. Zhang, S. F. Wang, M. Hu and Y. Xiao, *Biosens. Bioelectron.*, 2006, **21**, 2180–2186.
16 L. Shen and P. L. He, *Electrochem. Commun.*, 2007, **9**, 657–662.
17 G. Zhao, F. Xing and Sh. Deng, *Electrochem. Commun.*, 2007, **9**, 1263–1268.
18 G. Testa, L. Fontana, I. Venditti and I. Fratoddi, *Beilstein J. Nanotechnol.*, 2016, **7**, 1822.
19 G. Gerent and A. Spinelli, *J. Hazard. Mater.*, 2017, **330**, 105–115.
20 Q. Wang, C. Yang, Q. Yang, S. Yu and H. Yang, *Anal. Chim. Acta*, 2018, **1046**, 93–98.
21 M.-S. Ekrami-Kakhki, M. Khorasani-Motlagh and M. Noroozifar, *J. Appl. Electrochem.*, 2011, **41**, 527–534.
22 F. Kaedi, Z. Yavari, M. Noroozifar and H. Saravani, *J. Electroanal. Chem.*, 2018, **827**, 204–212.
23 A. S. Douk, H. Saravani and M. Noroozifar, *Int. J. Hydrogen Energy*, 2018, **43**, 7946–7955.
24 Z. Yavari, M. Noroozifar and M. Khorasani-Motlagh, *J. Appl. Electrochem.*, 2015, **45**, 439–451.
25 L. Wang and E. K. Wang, *Electrochem. Commun.*, 2004, **6**, 225–229.
26 S. Q. Liu, D. Leech and H. X. Ju, *Anal. Lett.*, 2003, **36**, 1–19.
27 M. Shahbakhsh and M. Noroozifar, *Biosens. Bioelectron.*, 2018, **102**, 439–448.
28 A. J. Bard, L. R. Faulkner, J. Leddy and C. G. Zoski, *Electrochemical methods: fundamentals and applications*, Wiley, New York, 1980.
29 V. Gau, S.-C. Ma, H. Wang, J. Tsukuda, J. Kibler and D. A. J. M. Haake, *Methods*, 2005, **37**, 73–83.
30 M. Tohidinia, M. Farsadrooh, S. Bahmanzadeh, N. Sabbaghi and M. J. R. A. Noroozifar, *RSC Adv.*, 2018, **8**, 1237–1245.
31 J. Liu, D. Takeshi, K. Sasaki and S. Lyth, *J. Electrochem. Soc.*, 2014, **161**, F838–F844.
32 M. Sharp, M. Petersson and K. Edström, *J. Electroanal. Chem.*, 1979, **95**, 123–130.
33 M. Tohidinia and M. Noroozifar, *Int. J. Electrochem. Sci.*, 2018, **13**, 2310–2328.
34 J. Velasco, *Electroanalysis*, 1997, **9**, 880–882.
35 C. Wu, Z. Liu, H. Sun, X. Wang and P. J. B. Xu, *Biosens. Bioelectron.*, 2016, **79**, 843–849.
36 P. Rattanarat, A. Suea-Ngam, N. Ruecha, W. Siangproh, C. S. Henry, M. Srisa-Art and O. Chailapakul, *Anal. Chim. Acta*, 2016, **925**, 51–60.
37 J. Gao, M. Liu, H. Song, S. Zhang, Y. Qian and A. Li, *J. Hazard. Mater.*, 2016, **318**, 99–108.
38 N. A. Penner and P. N. J. A. Nesterenko, *Analyst*, 2000, **125**, 1249–1254.
39 M. Zheng, Y. Wu, L. Lu, K. Ding, F. Tang, Z. Lin and X. Wu, *J. Sep. Sci.*, 2011, **34**, 2072–2078.
40 L. Y. Shiroma, M. Santhiago, A. L. Gobbi and L. Kubota, *Anal. Chim. Acta*, 2012, **725**, 44–50.
41 S.-P. Wang and T.-H. Huang, *Anal. Chim. Acta*, 2005, **534**, 207–214.
42 E. Wyszecka-Kaszuba, M. Warowna-Grześkiewicz and Z. Fijałek, *J. Pharm. Biomed. Anal.*, 2003, **32**, 1081–1086.
43 M. Zheng, Y. Wu, L. Lu, K. Ding, F. Tang, Z. Lin and X. Wu, *J. Sep. Sci.*, 2011, **34**, 2072–2078.